OPTICA ACTA, 1983, VOL. 30, NO. 1, 23–40

The shadows of floating objects and dissipating vortices

M. V. BERRY and J. V. HAJNAL
H. H. Wills Physics Laboratory, Royal Fort,
Tyndall Avenue, Bristol BS8 1TL, England

(*Received 19 May 1982*)

Abstract. The optical effects of gently deformed water surfaces are studied analytically for three examples: a straight floating edge, a small floating sphere and a dissipating free vortex. The surface deformation is obtained in the first two cases by solving Laplace's surface tension equation, and in the third case from the Bernoulli and Coriolis effects of a velocity field obtained from the Navier–Stokes equation. At small depths, a straight floating edge gives a normal shadow decorated by Fresnel fringes, but at greater depths the illuminated region is bounded by a caustic, giving a bright-edged shadow decorated with Airy-function fringes. A small floating sphere gives an approximately paraboloidal caustic decorated with bright Airy-function fringes (produced by the curved water surface), within which are faint Bessel-function fringes (produced by the ring of water bounding the sphere). A free vortex gives a caustic consisting of two roughly cylindrical sheets joined at a cusp-edged ring, whose section at a given depth consists of two concentric caustics bounding a bright annulus. The sphere and vortex theories are illustrated by experiments. All analytical results are expressed as universal functions whose dimensionless variables are related to the physical variables by scaling laws.

1. Introduction

Most people have noticed the sun-shadows cast on river beds by floating leaves and insects and by vortices which dissipate whilst drifting on the current. The distinctive form of these shadows is the result of refraction and diffraction by the water surface which is deformed under the influence of gravity and surface tension. In particular, the shadows often have bright edges which are caustics of light rays focused by the surface.

Our purpose here is to explain these phenomena by working out in detail the optics of three illustrative examples. The first is a floating object with a long straight edge, and is discussed in § 2. The second is a small floating sphere; the surface profile is obtained in § 3 and the consequent refraction and diffraction are studied in §§ 4 and 5. A brief description of an illustrative experiment is given in the Appendix. The final example is a floating vortex; the hydrodynamics and surface profile are obtained in § 6, and the refraction is considered in § 7.

What makes the theory tractable is the single approximation that the deformations of the water surface are gentle in the sense that they have small slopes. If the deformation is $f(\mathbf{r})$, measured downwards from the horizontal undeformed surface with coordinates $\mathbf{r} \equiv (x, y)$, then the approximation is

$$|\nabla f| \ll 1. \tag{1}$$

0030 3909/83/3001 0023 $04·00 © 1983 Taylor & Francis Ltd

This simplifies the determination of $f(\mathbf{r})$ because the total curvature is just $\nabla^2 f$, and Laplace's equation, equating the product of surface tension and curvature to the excess pressure, becomes linear. This equation is conveniently written as

$$\nabla^2 f(\mathbf{r}) = \frac{1}{L^2} f(\mathbf{r}), \tag{2}$$

where

$$L \equiv \sqrt{\left(\frac{\gamma}{dg}\right)} = 2{\cdot}73\,\text{mm} \tag{3}$$

is the 'surface tension length', and γ, d and g are the surface tension, water density and gravitational acceleration.

The other simplification resulting from equation (1) is that the optics is paraxial. If the light is incident normally there are two possible configurations, illustrated in figure 1: case A (common in nature) in which the light shines from above, and case B (convenient in experiments) in which the light shines from below. In both cases we choose coordinates Z, $\mathbf{R} \equiv (X, Y)$ in the refraction space, as shown. To construct the wavefunction $\psi(\mathbf{R}, Z)$ in the refraction space, we employ Kirchoff's integral which requires for its elementary wavelets the optical distance $S(\mathbf{r}; \mathbf{R}, Z)$ from a source at $\mathbf{r}$, $Z = 0$ to the field point $\mathbf{R}$, Z. If the water has refractive index μ, this distance is given by

case A:

$$\begin{aligned} S(\mathbf{r}; \mathbf{R}, Z) &= f(\mathbf{r}) + \mu\{[Z - f(\mathbf{r})]^2 + (\mathbf{R} - \mathbf{r})^2\}^{1/2} \\ &\approx \mu Z + \mu R^2/2Z - (\mu - 1) f(\mathbf{r}) + \mu(r^2 - 2\mathbf{R}\cdot\mathbf{r})/2Z, \end{aligned} \tag{4}$$

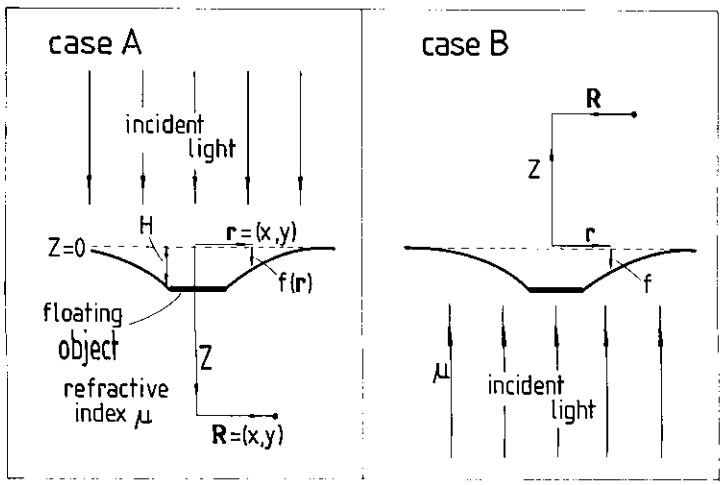

Figure 1. Geometry and coordinates for light incident from above (case A) and below (case B) the water surface.

case B:

$$S(\mathbf{r};\mathbf{R},Z)=-(\mu-1)f(\mathbf{r})+\{Z^2+(\mathbf{R}-\mathbf{r})^2\}^{1/2}$$
$$\approx Z+R^2/2Z-(\mu-1)f(\mathbf{r})+(r^2-2\mathbf{R}\cdot\mathbf{r})/2Z, \tag{5}$$

where the second term in each equation incorporates the paraxial approximation. We shall henceforth ignore the first two terms in S, which simply contribute an overall phase factor to ψ, and write the equations for case A only (those for case B can be obtained by multiplying Z by μ).

For light with wavenumber k ($=2\pi/\lambda$ where λ is the wavelength) and unit incident intensity, Kirchhoff's integral gives

$$\psi(\mathbf{R},Z)=\frac{k\mu}{2\pi iZ}\int\int_{\mathscr{R}} d\mathbf{r}\exp\{ik[-(\mu-1)f(\mathbf{r})+\mu(r^2-2\mathbf{r}\cdot\mathbf{R})/2Z]\}, \tag{6}$$

where $\mathscr{R}$ is the region of the water surface illuminating the refraction space (i.e. excluding floating objects).

At the level of geometrical optics, the ray(s) through $\mathbf{R},Z$ originate from the point(s) $\mathbf{r}$ for which $\nabla_{\mathbf{r}}S$ is zero (Fermat's principle). From equation (4), or by elementary reasoning, the resulting ray equation is

$$\mathbf{R}=\mathbf{r}-Z\left(1-\frac{1}{\mu}\right)f(\mathbf{r}). \tag{7}$$

The caustic is the focal surface (in the refraction space) on which S is stationary to higher than first order, and this implies (see, for example, Berry and Upstill [1] or Berry [2]) that $\mathbf{R},Z$ lies on a centre of curvature of the wavefront at $\mathbf{r}$, i.e.

$$Z^{-1}=\frac{[1-(1/\mu)]}{2}\{\nabla^2 f\pm[(f_{xx}-f_{yy})^2+4f_{xy}^2]^{1/2}\}, \tag{8}$$

where subscripts denote partial derivatives. The importance of the caustic surface lies in the fact that on it the light intensity is infinite in geometrical optics, and rises to high values (typically $O(k^{1/3})$) when diffraction is taken into account.

2. Straight floating edge

Let $x=0$ be the straight edge of an object (e.g. a razor blade) floating at a depth H. Then the surface deformation for $x\geqslant 0$, which must be independent of y, is given by the solution of equation (2) satisfying $f(x=0)=\mathrm{H}$ and $f(x\to\infty)\to 0$, namely

$$f(x)=H\exp(-x/L). \tag{9}$$

Our gentle-slope condition requires that $H\ll L$.

Using the dimensionless variables

$$\xi\equiv X/L,\quad s\equiv x/L,\quad \zeta\equiv ZH\left(1-\frac{1}{\mu}\right)\Big/L^2, \tag{10}$$

the ray and caustic equations (7) and (8) give

$$\xi=s+\zeta\exp(-s)\quad(s\geqslant 0) \tag{11}$$

and

$$\zeta=\exp(s). \tag{12}$$

These equations can be solved explicitly (by eliminating s) to give the caustic in the refraction space as

$$\zeta = \exp(\xi - 1) \quad (\xi > 1). \tag{13}$$

On the other hand, the shadow ray, from $x = s = 0$, is, from equation (11)

$$\zeta = \xi. \tag{14}$$

It follows (see figure 2) that only for $\zeta < 1$ does the shadow ray bound the illuminated region; for $\zeta > 1$ it is the caustic which separates the lit region from the dark region. Floating objects such as insects and leaves depress water surfaces by H values such that $\zeta = 1$ corresponds to a few centimetres, and that is why their shadows in water deeper than this have bright edges. By gently lifting a screen of paper in a pan of water on which a razor blade is floating (lit from above), the transition between bright-edged shadows ($\zeta > 1$) and normal shadows ($\zeta < 1$) is easily seen.

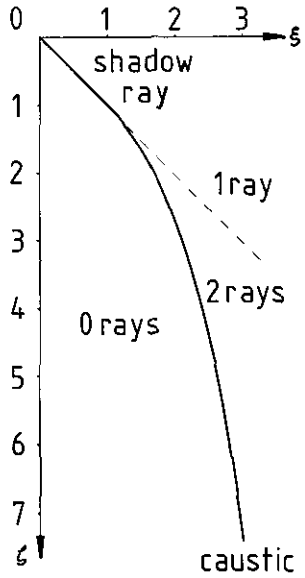

Figure 2. Shadow and caustic from straight floating edge.

Bright-edged caustic shadows occur only when the floating object depresses the water surface. If the surface is raised, it acts as a diverging lens and there are no real caustics, so that the shadows are normal. This is easily illustrated by lifting an illuminated razor blade just proud of the water surface. Another distinction between these two cases is the size of the shadow. When the water is depressed, the shadow is consistently larger than that which would result if the water surface were flat, and it increases in size with Z. On the other hand, when the surface is raised the shadow is smaller.

Diffraction phenomena associated with a straight floating edge are described by the Kirchhoff formula (6). Introducing the deformation (9), the variables (10) and the dimensionless wavenumber

$$\kappa \equiv kH(\mu-1), \tag{15}$$

and evaluating the trivial gaussian integral over y, we obtain

$$\psi(\xi,\zeta)=\exp(-i\pi/4)\left(\frac{\kappa}{2\pi\zeta}\right)^{1/2}\int_0^\infty ds\exp\{i\kappa[-\exp(-s)+(s^2-2s\xi)/2\zeta]\}. \tag{16}$$

We shall evaluate this integral in the asymptotic limit $\kappa\to\infty$ for which the diffraction effects associated with the two types of shadow ($\zeta>1$ and $\zeta>1$) are very different.

If $\zeta<1$, the integral is dominated by a single stationary point (ray) in the lit region $\xi>\zeta$, and by the end-point $s=0$ in the shadow $\xi<\zeta$. Near $\xi=\zeta$ the stationary point collides with the end-point, and expansion of the phase for small s leads to

$$\psi(\xi,\zeta)\approx\frac{\exp\left\{-i\kappa\left[1-\dfrac{(\xi-\zeta)^2}{2\zeta(1-\zeta)}\right]\right\}}{\sqrt{(1-\zeta)}}\,\Phi\left\{(\xi-\zeta)\left[\frac{\kappa}{2\zeta(1-\zeta)}\right]^{1/2}\right\} \tag{17}$$

$$(|\xi-\zeta|\ll\zeta,\quad \kappa\gg1,\quad \zeta<1),$$

where Φ denotes the Fresnel integral

$$\Phi(\tau)\equiv\frac{\exp(-i\pi/4)}{\sqrt{\pi}}\int_0^\infty dw\exp[i(w-\tau)^2], \tag{18}$$

which has the limiting forms

$$\Phi(\tau)\to\begin{cases}1 & (\tau\to+\infty)\\ \frac{1}{2} & (\tau=0)\\ \exp\left[i\left(\dfrac{\pi}{4}+\tau^2\right)\right]\Big/2|\tau|\sqrt{\pi} & (\tau\to-\infty).\end{cases} \tag{19}$$

On the shadow's edge, therefore, the wave intensity $|\psi|^2$ is

$$|\Psi(\xi=\zeta,\zeta)|^2\approx[4(1-\zeta)]^{-1}\quad(\zeta<1,\kappa\gg1), \tag{20}$$

which is independent of κ.

If $\zeta>1$, the integral is dominated by two real stationary points (rays) in the lit region $\xi>1+\ln\zeta$ (see equation (13)) and by two complex stationary points in the shadow $\xi<1+\ln\zeta$. Near the caustic at $\xi=1+\ln\zeta$, where the two stationary points collide, expansion of the phase of equation (16) for small $s-\ln\zeta$ (see equation (12)) leads to

$$\psi(\xi,\zeta)\approx\left(\frac{\kappa}{\zeta}\right)^{1/6}2^{5/6}\sqrt{\pi}\exp\left\{-i\left[\frac{\pi}{4}+\frac{\kappa}{\zeta}(1+\xi\ln\zeta)\right]\right\}$$

$$\times\mathrm{Ai}\left[-2^{1/3}\left(\frac{\kappa}{\zeta}\right)^{2/3}(\xi-1-\ln\zeta)\right]\quad(|\xi-1-\ln\zeta|\ll1,\kappa\gg1,\zeta>1), \tag{21}$$

where Ai denotes the Airy function (Abramowitz and Stegun [3])

$$\mathrm{Ai}(\tau)\equiv\frac{1}{2\pi}\int_{-\infty}^{\infty}dw\exp\left[i\left(\frac{w^3}{3}+\tau w\right)\right], \tag{22}$$

which has the limiting forms

$$\mathrm{Ai}(\tau)\to\begin{cases}\exp\left(-\frac{2}{3}\tau^{3/2}\right)\Big/2\tau^{1/4}\sqrt{\pi} & (\tau\to+\infty)\\ \Gamma\left(\frac{2}{3}\right)\Big/3^{2/3}=0{\cdot}35503 & (\tau=0)\\ \sin\left(\frac{2}{3}|\tau|^{3/2}+\frac{\pi}{4}\right)\Big/|\tau|^{1/4}\sqrt{\pi} & (\tau\to-\infty).\end{cases} \tag{23}$$

On the caustic, therefore, the wave intensity is

$$|\psi(\xi=1+\ln\zeta,\zeta)|^2\approx 2^{5/3}\pi\,\mathrm{Ai}^2(0)\,(\kappa/\zeta)^{1/3}=1{\cdot}257(\kappa/\zeta)^{1/3}\quad(\zeta>1,\kappa\gg1), \tag{24}$$

which diverges in the geometrical optics limit as $\kappa^{1/3}$.

As ζ increases through unity, there is a transition from Fresnel edge diffraction, described by equation (17), to Airy caustic diffraction, described by equation (21). The transition could be described by an 'incomplete Airy function'; we do not give details but point out that this is the simplest of the 'constraint diffraction catastrophes'.

3. Small floating sphere: surface deformation

Let the sphere have density d_0 and radius a_0, and let it be suspended from a circle of radius a (see figure 3) at depth H. Then the surface deformation, which must have circular symmetry, is given by the solution of equation (2) satisfying $f(a)=H$ and $f(|\mathbf{r}|\to\infty)\to0$, namely

$$f(r)=HK_0(r/L)/K_0(a/L), \tag{25}$$

where $r\equiv|\mathbf{r}|$ and K_0 denotes the zero-order modified Bessel function of the second kind (Abramowitz and Stegun [3]).

H is determined by the balance of vertical forces acting on the sphere:

$$\underset{\text{weight}}{\frac{4}{3}\pi d_0a_0^3g}=\underset{\text{surface tension}}{2\pi a\gamma(-f'(a))}+\underset{\substack{\text{fluid pressure}\\ \text{at depth } H}}{\pi a^2dgH}+\underset{\substack{\text{fluid pressure}\\ \text{from water displaced}\\ \text{below } H}}{\frac{4}{3}\pi da_0^3\eta g}, \tag{26}$$

where η is the fraction of the sphere lying below depth H. Using equation (25) for f' and equation (3) for γ gives

$$H=\frac{4a_0^3\left[\frac{d_0}{2d}\left(1-\frac{d\eta}{d_0}\right)\right]K_0(a/L)}{3aL|K_0'(a/L)|\left[1+\frac{aK_0(a/L)}{2L|K_0'(a/L)|}\right]}. \tag{27}$$

For spheres much smaller than the surface tension length,

$$K_0(a/L)\approx\ln(2L/a)-0{\cdot}57721\quad(a\ll L), \tag{28}$$

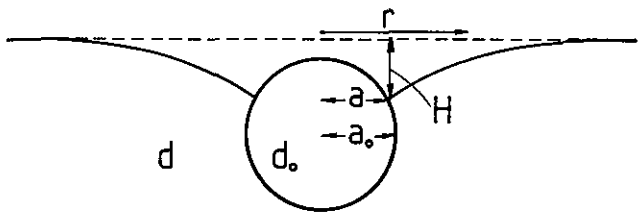

Figure 3. Geometry of floating sphere.

and the second term in the denominator of equation (27) is negligible. (In the experiments we performed—see §§4 and 5—the largest sphere had $a_0 = 0{\cdot}54$ mm and the term neglected was 0·034.) For glass spheres ($d_0 = 2640\,\mathrm{kg\,m^{-3}}$), the term in brackets in the numerator ranges from 1·32 when $\eta = 0$ (sphere almost clear of the surface) to 0·82 when $\eta = 1$ (sphere almost entirely submerged); we choose the value 1·07, corresponding to $\eta = 1/2$ (equatorial suspension, i.e. $a = a_0$). (Of course η and a/a_0 are not free parameters but depend on the contact angle between the sphere and the water surface—a quantity very sensitive to the precise conditions at the interface and notoriously difficult to measure.)

Thus H becomes, to a good approximation,

$$H = \frac{1{\cdot}427 a_0^3}{L^2} K_0(a/L). \tag{29}$$

For $a_0 = 0{\cdot}54$ mm this gives $H = 0{\cdot}052$ mm, so that the gentle-slope condition is well satisfied. From equation (25), the final formula for the surface profile becomes

$$f(r) = DK_0(r/L), \tag{30}$$

where

$$D = 1{\cdot}427 a_0^3/L^2. \tag{31}$$

4. Small floating sphere: refraction

The caustic obviously has circular symmetry in the refraction space, and so depends only on $R \equiv |\mathbf{R}|$ and Z. Defining the dimensionless variables (see equations (10) for the straight floating edge)

$$\rho \equiv R/L, \quad s \equiv r/L, \quad \zeta \equiv ZD[1 - (1/\mu)]/L^2, \tag{32}$$

equations (7) and (8) give the caustic parametrically as $\rho = \rho_c$, $\zeta = \zeta_c$, where

$$\rho_c = s - K_0'(s)/K_0''(s) \tag{33}$$

and

$$\zeta_c = 1/K_0''(s). \tag{34}$$

Figure 4 shows the caustic (which resembles a deformed paraboloid) as computed using tables of Bessel functions. The parameter s can be eliminated from small and large ρ, giving the explicit limiting forms

$$\zeta_c \to \begin{cases} \rho_c^2/4 & (\rho_c \ll 1) \\ \left[\dfrac{2(\rho_c - 1)}{\pi}\right]^{1/2} \exp(\rho_c - 1) & (\rho_c \gg 1). \end{cases} \tag{35}$$

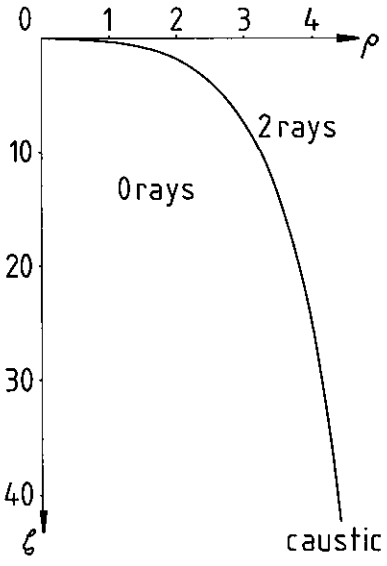

Figure 4. Section through computed caustic from small floating sphere.

Whatever the sphere's values of a_0, d_0 and a, its caustic should be given by the 'universal' formulae (33) and (34) after the scaling (32). We have tested this by experiment (appendix A) by illuminating small floating glass spheres from below (case B of figure 1) with collimated laser light and measuring the radius R_c of the caustic as a function of height Z above the water surface. For each value of $\rho_c = R_c/L$, ζ_c was computed from equations (33) and (34) (see figure 4) and plotted against the measured values of Z. The result should be a straight line with slope given by equations (32) and (31) as

$$\frac{d\zeta}{dZ} = \frac{1{\cdot}427 a_0^3}{L^4}(\mu - 1). \tag{36}$$

Figure 5 shows the resulting graph of ζ_c versus Z for a sphere with radius $a_0 = 0{\cdot}35$ mm. The best-fit straight line has slope $0{\cdot}28\,\mathrm{m}^{-1}$, whereas equation (36) predicts that $d\zeta/dZ = 0{\cdot}37\,\mathrm{m}^{-1}$ for this case. For a sphere of radius $a_0 = 0{\cdot}54$ mm, the graph was again accurately linear, with slope $1{\cdot}20\,\mathrm{m}^{-1}$ as compared with $d\zeta/dZ = 1{\cdot}36\,\mathrm{m}^{-1}$ predicted by equation (36). In view of the uncertainty about the submerged fraction η discussed below equation (28), we consider that this is good agreement. For a sphere of radius $a_0 = 0{\cdot}12$ mm, a straight line was again obtained, but the slope $0{\cdot}034\,\mathrm{m}^{-1}$ compared poorly with the predicted value of $0{\cdot}015\,\mathrm{m}^{-1}$. However, this sphere is so small that the depth H of the 'dimple' it produces is only $1{\cdot}7\lambda$, which is probably too small to justify any theory neglecting diffraction.

5. Small floating sphere: diffraction

The diffracted wave ψ is the Kirchhoff integral (6) with f given by equation (30) and the domain $\mathscr{R}$ consisting of the region $r > a$ not excluded by the sphere. Employing the dimensionless variables (32), also scaling k and a using

$$\kappa \equiv kD(\mu - 1) \quad \text{and} \quad \alpha \equiv a/L, \tag{37}$$

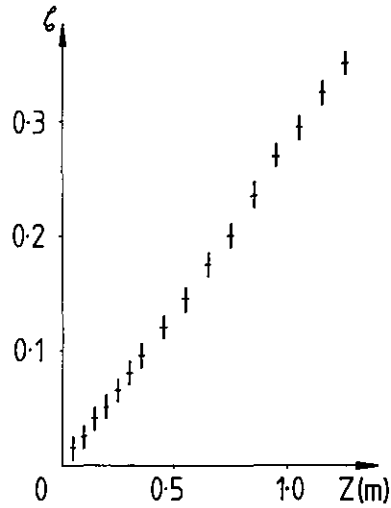

Figure 5. Graph of ζ_c (computed from measured caustic radius R_c) against distance Z from the screen, for a floating glass sphere of radius 0·35 mm.

and evaluating the angular integral in **r** space, we obtain

$$\psi(\rho,\zeta)=\frac{\kappa}{i\zeta}\int_{\alpha}^{\infty} ds\, s \exp\left\{i\kappa\left[\frac{s^2}{2\zeta}-K_0(s)\right]\right\} J_0\left(\frac{\kappa s\rho}{\zeta}\right), \tag{38}$$

where J_0 denotes the zero-order Bessel function of the first kind.

Now we make use of the fact that α is small and κ large to effect a separation of the integral into two parts, corresponding physically to diffraction by the water boundary $r=a$ and diffraction by the curved surface (which is dominated by the caustic). This can be achieved provided the Bessel factor is oscillating more slowly than the exponential factor at the lower limit $s=\alpha$, i.e. provided

$$\frac{d}{ds}\left(\frac{s\rho}{\zeta}\right)=\frac{\rho}{\zeta}<\frac{d}{ds}\left(\frac{s^2}{2\zeta}-K_0(s)\right)_{s=\alpha}=\frac{1}{\alpha}+\frac{\alpha}{\zeta}. \tag{39}$$

For all cases of interest here, this inequality is satisfied even if ρ lies on the caustic. Therefore the contribution to equation (38) from the rapid variation of the exponential factor at the lower limit can be extracted by integrating by parts, and gives ψ as the sum of two waves:

$$\psi(\rho,\zeta)=\psi_B(\rho,\zeta)+\psi_C(\rho,\zeta) \tag{40}$$

where

$$\psi_B(\rho,\zeta)=\frac{\alpha}{\zeta[1+(\alpha^2/\zeta)]} J_0\left(\frac{\kappa\rho\alpha}{\zeta}\right)\exp\left\{i\kappa\left[\frac{\alpha^2}{2\zeta}-K_0(\alpha)\right]\right\} \tag{41}$$

and

$$\psi_c(\rho,\zeta)=\frac{\kappa}{i\zeta}\int_{0}^{\infty} ds\, s \exp\left\{i\kappa\left[\frac{s^2}{2\zeta}-K_0(s)\right]\right\} J_0\left(\frac{\kappa\rho s}{\zeta}\right). \tag{42}$$

The wave ψ_B arises from diffraction by the ring of water immediately adjacent to the sphere, and its analytic form involving $J_0(w)$ is to be distinguished from the more familiar 'Airy-disc' obstacle diffraction involving $J_1(w)/w$. Figure 6 shows a comparison of the intensities corresponding to these two functions; note that J_0^2 decays more slowly, so that we expect to see many more rings with this kind of diffraction (as illustrated in the central region of figure 7).

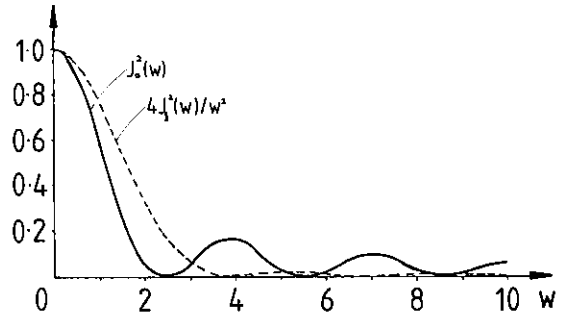

Figure 6. Comparison of water boundary diffraction intensity $J_0^2(w)$ (full line) with obstacle diffraction (Airy-disc) intensity $4J_1^2(w)/w^2$ (dashed line).

The wave ψ_c arises from diffraction from the curved water surface and is dominated by the caustic. To understand these effects we first replace J_0 in equation (42) by its asymptotic form for large argument, namely

$$J_0(w) \approx \frac{1}{\sqrt{(2\pi w)}} \{\exp[i(w-\pi/4)] + \exp[-i(w-\pi/4)]\}, \tag{43}$$

this procedure being justified because κ is assumed large. The first of these asymptotic terms gives, when substituted into equation (42), an integrand oscillating without stationary points along its whole range $0 \leqslant s \leqslant \infty$. Therefore it can be neglected in comparison with the second term, which has two stationary points coalescing at the caustic $\rho = \rho_c$ given by equations (33) and (34). The resulting oscillatory integral can be evaluated near the caustic by expanding its phase up to third order in $s - s_c$, where s_c is the solution of equation (34), i.e. the s value contributing to the caustic at depth ζ. This procedure leads to

$$\psi_c(\rho, \zeta) \approx \frac{\kappa^{1/6}}{|K_0''(s_c)|^{1/3}} \left(\frac{\pi s_c}{\zeta \rho_c}\right)^{1/2} 2^{5/6} \exp\left(-i\left\{\frac{\pi}{4} + \kappa\left[K_0(s_c) + \frac{\rho s_c}{\zeta} - \frac{s_c^2}{2\zeta}\right]\right\}\right) \times \mathrm{Ai}\left[-\frac{2^{1/3}\kappa^{2/3}}{\zeta |K_0''(s_c)|^{1/3}}(\rho - \rho_c)\right], \tag{44}$$

which should be compared with the 'straight-edge' result (21), with which it is identical apart from a phase if $\zeta \gg 1$.

The picture emerging from this analysis of the diffraction at depth ζ is of central 'Bessel' rings surrounded by the caustic at ρ_c, which for $\rho > \rho_c$ is decorated by 'Airy' fringes (not to be confused with the 'Airy disc' which, as stated above, plays no part

in this theory). Of the two features, the caustic is much the dominant. To see this we compare the intensity on the caustic, namely

$$|\psi_c(\rho_c, \zeta_c)|^2 = \frac{\kappa^{1/3} s_c}{|K_0''(s_c)|^{2/3} \zeta_c \rho_c} 2^{5/3} \pi \operatorname{Ai}^2(0) = \frac{1{\cdot}2572 \kappa^{1/3} s_c}{\zeta_c \rho_c |K_0'''|^{2/3}}$$

$$\rightarrow \begin{cases} 0{\cdot}3960 \kappa^{1/3} & (\zeta \ll 1) \\ 1{\cdot}2572 \left(\dfrac{\kappa}{\zeta_c}\right)^{1/3} & (\zeta \gg 1), \end{cases} \tag{45}$$

with the central 'Bessel' intensity, namely

$$|\psi_B(0, \zeta)|^2 = \alpha^4 / \zeta^2 \tag{46}$$

It is clear that $|\psi_c(\rho_c, \zeta)|^2$ greatly exceeds $|\psi_B(0, \zeta)|^2$ when, as we assume, α is small and κ is large, unless ζ is very small.

Now we compare the dimensions of the two sorts of fringe. The radius ρ_B of the first Bessel intensity maximum in the ring surrounding the central peak (corresponding to $J_0(3{\cdot}832)$) is, from equation (41),

$$\rho_B = \frac{3{\cdot}832 \zeta}{\kappa \alpha}. \tag{47}$$

The separation $\Delta\rho$ of the first two Airy intensity minima (i.e. dark fringes, corresponding to $\operatorname{Ai}(-2{\cdot}338$ and $\operatorname{Ai}(-4{\cdot}088))$ is, from equation (44),

$$\Delta\rho = \frac{1{\cdot}389 \zeta |K_0'''(s_c)|^{1/3}}{\kappa^{2/3}} \rightarrow \begin{cases} \dfrac{1{\cdot}750 \zeta^{1/2}}{\kappa^{2/3}} & (\zeta \ll 1) \\ 1{\cdot}389 (\zeta/\kappa)^{2/3} & (\zeta \gg 1). \end{cases} \tag{48}$$

It is clear from these formulae that $\Delta\rho/\rho_B \sim \kappa^{1/3}$ as $\kappa \rightarrow \infty$, so that the caustic fringes dominate in spacing as well as intensity (at least while $\zeta < 0{\cdot}048 \alpha^3 \kappa$).

These structures in the fully developed diffraction pattern are illustrated in figure 7, which is a photograph of the shadow from a glass sphere of radius $a_0 = 0{\cdot}34$ mm illuminated with laser light of wavelength $\lambda = 633$ nm (for experimental details see the Appendix). Equations (37) and (31) give $\kappa = 24{\cdot}8$, which is large enough to expect ray effects to dominate. And indeed the caustic, decorated with its Airy fringes, is evident. Near the centre of the photograph the Bessel rings can also be seen.

To make a rough quantitative comparison between experiment and theory, note first that figure 7 corresponds to an image plane whose distance from the water surface is $z = 95$ mm, so that from equations (32) and (31) $\zeta = 0{\cdot}032$. According to equations (35), the dimensionless caustic radius at this depth is $\rho_c = 0{\cdot}357$. The ratio of Bessel ring radius to caustic radius is predicted from equations (47) to be $\rho_B/\rho_c = 0{\cdot}11$, whereas measurement gives 0·10. The ratio of Airy fringe spacing to caustic radius is predicted from equations (48) for small ζ to be $\Delta\rho/\rho_c = 0{\cdot}875/\kappa^{2/3}$, which is independent of ζ, and observation bears this out. However, the predicted value of this ratio, namely 0·103, is discordant with the measured value of 0·14. We think this discrepancy stems from our wish to display both sorts of diffraction simultaneously, i.e. with comparable intensity (equations (45) and (46) give 4·1 for the caustic : Bessel intensity ratio); and in this case one of the stationary-phase points

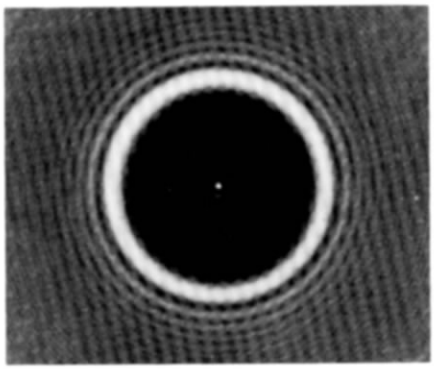

Figure 7. Diffraction pattern from a glass sphere of radius $a_0 = 0{\cdot}34$ mm, at a distance 95 mm from the water surface. The caustic and its Airy fringes dominate the image; the faint central rings are the Bessel fringes. (In order to remove image noise the photographic paper was rotated during printing.)

contributing to the diffraction near the caustic can stray close to, or even beyond, the end-point $s = \alpha$ of the integral (38). For a larger sphere ($a_0 = 0{\cdot}54$ mm), in a situation where the Bessel fringes were insignificant, the agreement was much better. Evidently all features observed can be accounted for by the theory to within the limits imposed by the uncertainty just discussed, and by the uncertainty in the fraction of the sphere submerged.

We remark that, although the theory was formulated for opaque spheres, our use of transparent spheres in experiments appears to have had no effect. This is because light transmitted by the sphere makes significant contributions only at (focal) distances $Z \sim a_0$, whereas we are concerned with effects occurring at much greater Z.

6. Dissipating vortex: surface deformation

We seek the deformation f of the free surface of a swirling liquid, that is a liquid whose velocity $\mathbf{u}$ at any point is horizontal and perpendicular to the line joining the point to a vertical symmetry line which we take as the Z axis. We shall determine f after solving the Navier–Stokes equation for $\mathbf{u}$ on the assumption that the speed $u(r, t)$ depends on $r = |\mathbf{r}|$ and time t, but not on Z.

The Navier–Stokes equation is

$$\frac{\partial \mathbf{u}}{\partial t} + \mathbf{u} \cdot \nabla \mathbf{u} = \nu \nabla^2 \mathbf{u} - \frac{\nabla p}{d} + \mathbf{g}, \tag{49}$$

where ν and d are the kinematic viscosity and density of the liquid, $\mathbf{g}$ is the gravitational acceleration and p is the pressure. To solve this we introduce the vorticity $\omega(r, t)$, defined by

$$\omega = \frac{1}{2}(\nabla \wedge \mathbf{u})_Z = \frac{1}{2r}\frac{\partial}{\partial r}(ru). \tag{50}$$

After taking the curl of equation (49), a little analysis leads to

$$\frac{\partial\omega}{\partial t}(r,t)=\nu\nabla^2\omega(r,t)=\frac{\nu}{r}\frac{\partial}{\partial r}\left(r\frac{\partial\omega}{\partial r}(r,t)\right). \tag{51}$$

The solution we shall use is

$$\omega(r,t)=\frac{C}{2\pi D^2(t)}\exp\left[-r^2/D^2(t)\right], \tag{52}$$

where

$$D^2(t)=r_0^2+4\nu t \tag{53}$$

and r_0 and C are constants. This describes a cylindrical gaussian concentration of vorticity which diffuses outwards from its initial radius r_0 under the action of viscosity.

From equation (50), the flow speed is

$$\begin{aligned}u(r,t)&=\frac{2}{r}\int_0^r dr'\,r'\omega(r',t)\\&=\frac{C}{2\pi r}\{1-\exp\left[-r^2/D^2(t)\right]\}.\end{aligned} \tag{54}$$

At distances $r\gg D(t)$, the flow is that of an irrotational vortex with circulation C, but the fact that for smaller r the vortex has a rotational core crucially affects the optics.

The surface profile depends on the pressure p; this is obtained by solving equation (49). The Z dependence of p is determined by $\mathbf{g}$, and the r dependence by the terms involving $\mathbf{u}$. Some analysis gives

$$p(r,Z,t)=dgZ-\frac{d}{2}u^2(r,t)-2d\int_r^\infty dr'\,u(r',t)\omega(r',t)+p_0, \tag{55}$$

where p_0 is the reference pressure at $Z=0$, $r\to\infty$.

Applying this formula to a point $Z=f(r,t)$ just below the surface, and equating the pressure difference to γ times the total curvature (see equation (2)), we obtain the equation governing the surface deformation as

$$L^2\nabla^2 f=\frac{L^2}{r}\frac{\partial}{\partial r}\left(r\frac{\partial f}{\partial r}\right)=f-\frac{1}{2g}\left[u^2+4\int_r^\infty dr'\,u(r',t)\omega(r',t)\right]. \tag{56}$$

The 'size' of the vortex may be taken as $D(t)$, and the surface-tension term is thus of the order of fL^2/D^2. As t increases, so does D, and this term becomes smaller. To quantify this effect, we note from equation (53) that the time t_2 for a vortex to double its radius is

$$t_2=\frac{3r_0^2}{4\nu} \tag{57}$$

For water, $\nu=10^{-6}\,\mathrm{m^2\,s^{-1}}$, so a vortex whose initial size is $r_0=L=2{\cdot}73$ mm doubles its size in $t_2=5{\cdot}6\,s$. Therefore the effect of surface tension soon becomes negligible, and the deformation is determined by Bernoulli and Coriolis effects. From this we obtain

$$f(r,t)=\frac{1}{2g}\left[u^2(r,t)+4\int_r^\infty dr'\,u(r',t)\omega(r',t)\right]. \tag{58}$$

Introducing the quantities

$$s \equiv \frac{r}{D(t)}, \quad H(t) \equiv \frac{C^2}{8\pi^2 D^2(t) g}, \tag{59}$$

and using equations (52) and (54), we finally obtain the deformation as

$$f(r, t) = HF(s), \tag{60}$$

where

$$F(s) = \frac{1}{s^2}[1 - \exp(-s^2)]^2 + 4\int_s^\infty \frac{ds'}{s'}[1 - \exp(-s'^2)]\exp(-s'^2)$$

$$= \frac{1}{s^2}[1 - \exp(-s^2)]^2 + 2[E_1(s^2) - E_1(2s^2)], \tag{61}$$

where E_1 denotes the exponential-integral function (Abramowitz and Stegun [3]). This universal function which with equations (59) describe the surface profile of the spreading vortex is depicted in figure 8. It has the following useful properties:

Asymptotics

$$F(s) \approx \begin{cases} 2\ln 2 - s^2 & (s \text{ small}) \\ \dfrac{1}{s^2} & (s \text{ large}), \end{cases} \tag{62}$$

Inflection

$$F''(s_i) = 0 \quad \text{where} \quad \frac{\exp(s_i^2)}{1 + (4s_i^2/3)} = 1, \quad \text{i.e.} \quad s_i = 0{\cdot}742,$$
$$F'(s_i) = -0{\cdot}877, \tag{63}$$

Stationary curvature

$$\left.\begin{aligned} &F'''(s_c) = 0 \qquad \text{where} \quad s_c = 1{\cdot}261, \\ &F''(s_c) = 0{\cdot}687, \\ &F'(s_c) = -0{\cdot}632 \end{aligned}\right\} \tag{64}$$

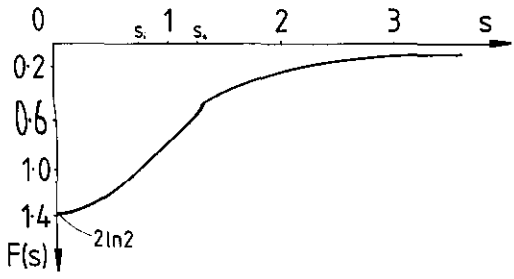

Figure 8. Universal surface profile (equation (61)) for dissipating vortex.

7. Dissipating vortex: refraction

The caustic of refracted rays is obtained from the refraction equations (7) and (8) using the surface deformation (60) and (61). Introducing dimensionless variables in the refraction space,

$$\rho \equiv \frac{R}{D(t)}, \quad \zeta \equiv \frac{Z(1-(1/\mu)]H(t)}{D^2(t)}, \tag{65}$$

we obtain the caustic curve in parametric form as

$$\left.\begin{aligned} \rho_c &= s - F'(s)/F''(s), \\ \zeta_c &= 1/F''(s), \end{aligned}\right\} \tag{66}$$

where s varies from 0 to ∞. Figure 9 shows the caustic. Its most striking feature is a cusp at $\zeta_{cusp}=1{\cdot}455$, $\rho_{cusp}=2{\cdot}181$.

To obtain the full caustic in space, figure 9 must be rotated about the ζ axis. This gives two surfaces joined at a cusped-edge ring. Sections of constant ζ exceeding ζ_{cusp} have two concentric circular caustics containing an annulus of bright light. We have observed caustics from vortices made by briefly rotating a bar magnet resting on the bottom of a cylindrical water tank with the aid of a spinning magnet brought up close below the tank. Figure 10 shows one such caustic; it evidently does have the predicted concentric form.

As time elapses the vortex spreads, and the evolution of its caustic is determined by the time-dependent scaling (65). In view of equations (59) and (53), this implies that the caustic swells horizontally (radius $\sim t^{1/2}$) whilst receding rapidly from the surface (cusp distance $\sim t^2$). In particular, the shadow disappears abruptly as the cusped ring passes the bottom of the tank or pool.

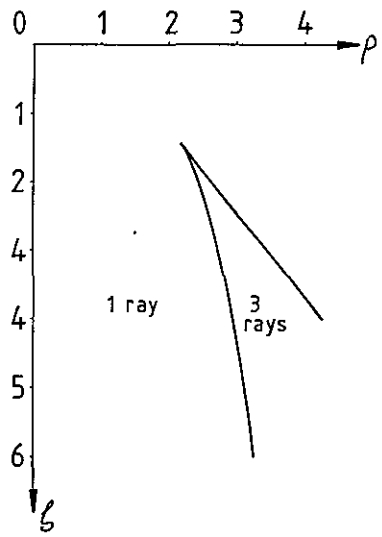

Figure 9. Universal caustic from dissipating vortex, calculated from equation (66).

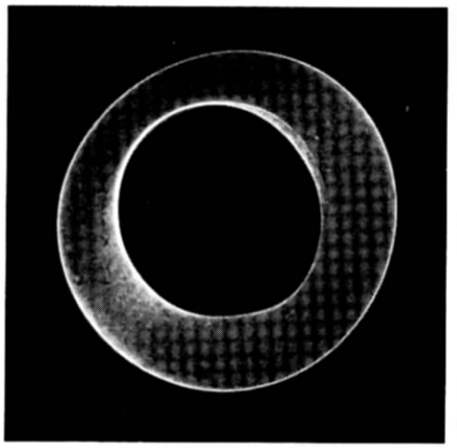

Figure 10. Section of caustic from dissipating vortex.

8. Conclusion

This work began with the desire to understand certain blemishes on images produced by curved water surfaces in studies of catastrophe optics. These blemishes consisted of small faint concentric rings and can be seen, for example in figure 5 of the paper by Nye [4] and figures 4 and C1 (*d*) of the paper by Upstill *et al.* [5]. We thought that they were caused by dust specks producing minute refracting dimples on the surface on scales much smaller than that of the droplets or waves being investigated, and inspection of the blemishes shows that the theory and experiments reported here support this interpretation.

Finally, note that the gentle-slope approximation (1) enabled us to work out the theory in full analytical detail: for each of the three problems (straight edge, sphere and vortex), the solutions for surface deformation, refraction and diffraction are expressed as universal functions whose dimensionless variables can be translated into physical variables by scaling. The two diffraction functions (16) and (42) differ in an important respect from the structurally stable diffraction functions of catastrophe theory [1, 2]—the fact that the phases of the integrands involve transcendental functions rather than polynomials means that the dimensionless wavenumber κ cannot be eliminated by scaling, whereas for the diffraction catastrophes it can. (In physical terms, the shadow patterns for different wavelengths are essentially different, and cannot be related by scaling.)

Acknowledgment

J. V. H. was supported by an SERC research studentship. This work was not supported by any military agency.

Appendix

Experimental details

The optical arrangement, as summarized in § 4 (case B of figure 1), consisted of floating spheres illuminated from below with collimated laser light ($\lambda = 633$ nm) which passed through the transparent base of a small water tank. It was found that

mechanical vibrations transmitted to the tank via the laboratory floor disturbed the water surface sufficiently to disrupt the diffraction patterns. The water tank was therefore mounted on a vibration-free support, as illustrated in figure 11. This consisted of a steel slab suspended on four wires from a frame secured to the upper tier of a table made from concrete slabs resting on pneumatic tyres. No single element of this system was by itself sufficient to ensure the necessary mechanical decoupling.

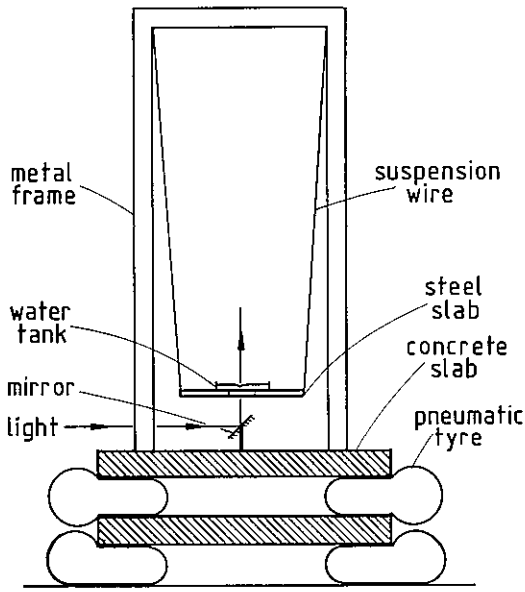

Figure 11. Vibration-free support for water tank.

An optical microscope with calibrated eyepiece was employed to measure the glass spheres. They were found to be spherical to within 0·5 per cent. The spheres were placed on the water surface with the aid of tweezers or, for the smaller spheres, a loop of human hair.

Windshields were provided to prevent gusts of air from disturbing the spheres. The resulting caustics and diffraction patterns were photographed through a microscope (providing a linear enlargement factor of ~ 6) which was focused on the appropriate plane in the refraction space.

Observations made in this way are discussed in §§ 4 and 5.

Les effets optiques de surfaces d'eau légèrement déformées sont étudiés analytiquement pour trois exemples: un coin flottant, une petite sphère flottante et un tourbillon libre qui se dissipe. La déformation de surface est obtenue, dans les deux premiers cas, en résolvant l'équation de tension de surface de Laplace et, dans le troisième cas, à partir des effets Bernouilli et Coriolis d'un champ de vitesse, par l'équation de Navier–Stokes. Un coin flottant donne, à faible profondeur, une ombre normale entourée de franges de Fresnel, mais, à plus grande profondeur, la région éclairée est limitée par une caustique, donnant une ombre bordée de lumière soulignée par des franges de fonction d'Airy. Une petite sphère flottante donne une caustique approximativement parabolique avec des franges brillantes de fonction d'Airy (produites par la surface de l'eau incurvée), à l'intérieur desquelles apparaissent de faibles

franges de fonction de Bessel (produites par l'anneau d'eau limitant la sphère). Un tourbillon libre donne une caustique consistant en deux nappes à peu près cylindriques reliées à un anneau avec point de rebroussement, dont la section, à une profondeur donnée, consiste en deux caustiques concentriques limitées par un anneau brillant. Les théories pour la sphère et le tourbillon sont illustrées par des expériences. Tous les résultats analytiques sont exprimés comme des fonctions universelles dont les variables sans dimensions sont reliées aux variables physiques par des lois d'échelle.

Die optischen Effekte von leicht deformierten Wasseroberflächen werden an drei Beispielen analytisch untersucht: eine gerade schwimmende Kante, eine kleine schwimmende Kugel und ein dissipierender freier Wirbel. Die Oberflächendeformation erhalten wir in den ersten beiden Fällen durch die Lösung der Laplaceschen Gleichung der Oberflächenspannung und im dritten Fall aus den Bernoulli- und Coriolis-Effekten eines Geschwindigkeitsfelds der Navier-Stokes–Gleichung. Eine gerade schwimmende Kante ergibt bei kleiner Tiefe einen normalen Schatten, der von Fresnel-Streifen verziert ist, bei größerer Tiefe wird die beleuchtete Region allerdings durch eine Kaustik begrenzt, wobei ein hell abgegrenzter Schatten mit Airy-Streifen entsteht. Eine kleine schwimmende Kugel ergibt eine annähernd parabolische Kaustik, verziert mit hellen Airy-Streifen (erzeugt durch die gekrümmte Wasseroberfläche), und schwächeren Bessel-Streifen (erzeugt durch den die Kugel begrenzenden Wasserring). Ein freier Wirbel ergibt eine Kaustik bestehend aus zwei fast zylindrischen Blättern, die in einem Scheitel zusammentreffen und deren Querschnitt bei einer bestimmten Tiefe aus zwei konzentrischen Kaustiken besteht, die einen hellen Ring begrenzen. Die Theorien zur Kugel und zum Wirbel werden durch Experimente illustriert. Alle analytischen Ergebnisse werden als universelle Funktionen ausgedrückt, deren dimensionslose Variablen mit den physikalischen Variablen durch Skalierungsgesetze in Verbindung stehen.

References

[1] Berry, M. V., and Upstill, C., 1980, *Progress in Optics*, edited by E. Wolf, Vol. 18 (Amsterdam: North-Holland), pp. 257–346.

[2] Berry, M. V., 1981, *Singularities in Waves and Rays*, edited by R. Balian, M. Kléman and J. P. Poirier (Amsterdam: North-Holland), pp. 454–543.

[3] Abramowitz, M., and Stegun, I. A., 1964, *Handbook of Mathematical Functions* (Washington, D.C.: National Bureau of Standards).

[4] Nye, J. F., 1978, *Proc. R. Soc.* A, **361**, 21–41.

[5] Upstill, C., Wright, F. J., Hajnal, J. V., and Templer, R. H., 1982, *Optica Acta*, **29**, 1651–1676.